A novel, fast readout, gamma detectorsystem for nuclear fingerprinting

A. Giroletti, J.J. Velthuis, T. Scott

Abstract—Decommissioning of legacy nuclear facilities or clean up in the aftermath of a nuclear incident requires a detailed knowledge of the amount, type and distribution of nuclear materials present. One technique available to rapidly provide this information in situ is high precision gamma spectroscopy. These spectrometers rely on precision measurements of energy deposited into the spectrometer from incident photons, however the high precision limits the speed of the measurements and therefore limits the upper threshold of radiation levels that can be measured. In this work we present the results from simulation of a novel, multi-detector system with a fast readout that is suitable for higher radiation levels.

1 Introduction

After a nuclear incident, such as the Fukushima Daiichi Nuclear Power Plant (FDNPP) accident, or during the decommissioning of legacy nuclear facilities, it is important to have the best possible understanding of the identity and concentration distribution of radionuclides present in the area or facility of interest. There are several techniques that can provide such information, with one of the most common non-destructive techniques being gamma spectroscopy. These devices require high precision measurements of the deposited energy to identify the radioisotopes present. These high precision measurements of single pulse (single photon interaction) events involve long shaping times which limits the maximum count rate and therefore the maximum radiation level that can be accurately measured. Overcoming this challenge and allowing the measurements of higher levels of radiation would be beneficial for monitoring in more extreme environments, such as those described above. Additionally, due to the small size and weight of the devices it allows their use on Unmanned Aerial Vehicles (UAVs), submersible Remotely Operated Vehicles (ROVs) or other unmanned platforms so that operator radiation exposure levels are limited or altogether avoided.

2 The concept

The photon interaction cross section for an impacted material is dependent on the energy of the incident photon and the electron density of the material it is interacting with: the absorbing material. A representative illustration for carbon and lead is shown in figure 1.

Our proposed device uses a matrix of detectors of five different materials: Silicon, Gallium Arsenide (GaAs), Uranium Oxide (UO_2), Cadmium Zinc Telluride (CZT) and Diamond. These detector materials were selected as they can all be operated at room temperature with no requirement for active cooling, allowing them to be assembled as part of a compact and lightweight detection system. Each of the five detectors has unique properties that allow a specific challenge to be overcome ([2], [4], [8]) and these are discussed below and presented in Table 1:

Silicon has moderate intrinsic charge concentration and intrinsic resistivity as well as being a low cost material. These features have led to its widespread use as a detector with a significant associated accumulation of information on how to adapt this material to gain the best performance for a specific application e.g. impurity doping. Due to its widespread use, its integration with a readout system is trivial ([8]).

GaAs is a dense material (5.32 g/cm^3) and therefore has good stopping power for incident photons in comparison to silicon. It also has a higher electron mobility and resistivity than silicon allowing the application of a higher electric field. These properties also allow the detector to be thicker than Silicon thereby enabling the full potential of its stopping power to be achieved ([8]).

UO_2 is a very high density material (10.97g/cm^3) that is inherently radioactive. This allows it to be used as a self-calibrating detector. Due its considerable stopping power on account of its density, it is ideally suited for detection of high energy gamma rays. An additional side benefit to using UO2 is that it also has neutron detection capabilities depending upon the isotopes of uranium from which the detection crystal is made ([10], [7]).

CZT is an established gamma radiation detector material which has a high bulk resistivity and low leakage current. It has been shown to be ideally suited for spectroscopic measurements due to its high detection efficiency, high resolution, temperature stability and relative low cost ([8]).

Diamond is a chemically inert and radiation hard material. Detector diamond is manufactured using chemical vapour deposition (CVD) to produce high quality, low impurity crystals that have very low leakage current. The main advantage of the diamond detector is its high radiation tolerance, allowing its use in extreme environments that may saturate other detectors ([8]).

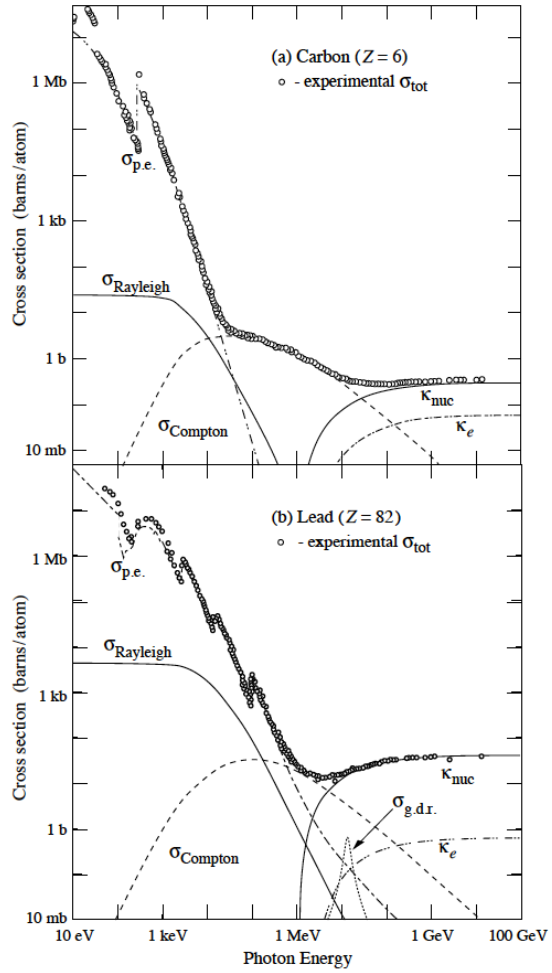

Fig. 1. Photon total cross sections as a function of energy in carbon and lead, showing the contributions of different processes. Taken from [6].

Material	Si	Diamond	CdZnTe	UO_2	GaAs
Density (g/cm^{-3})	2.329	3.52	5.78	10.97	5.32
Band Gap eV	1.1	5.5	1.56	1.30	1.42
ϵ (eV)	3.62	13	5.65	4.25	4.61
electron mobility μ_e $(cm^2V^{-1}s^{-1})$	1500	2000	1350		8500
hole mobility μ_h $(cm^2V^{-1}s^{-1})$	480	1600	120		400
bias voltage V	100-500	100-500	5-50		
leakage current	mA	pA	1-100 nA	μm	
Z	14	6	48-30-52	92-8	31-33

TABLE 1
Comparison of different semiconductors properties: density, bandgap and energy required to create an electron hole pair ([8], [10].)

When a photon interacts with a material, it deposits a specific amount of energy into the material. In a semiconductor material this leads to the production of a certain number of electron-hole pairs which when connected as part of a device (via opposing electrodes) are exploited to measure a small current pulse. The electron-hole pairs are caused by a number of different possible interactions, each generating a specific number of electron-hole pairs. These are the Photoelectric Effect, Compton Scattering and Pair Production (greater than 1022 keV) and these are discussed in detail below:

- **Photoelectric effect**: this is the absorbtion of a photon by an atomic electron which causes the emission of an electron from the atom that can interact with the detector. The energy of the emitted electron is given by:

$$E = h\nu - B.E. \tag{1}$$

  where B.E. is the electron binding energy.
  The photoelectric cross section is proportional to:

$$\sigma_{photo} \propto Z^5 \tag{2}$$

  where Z is the material atomic number.
- **Compton scattering**: This is the scattering of the incident photon and a free electron.
  The Compton scattering cross section is proportional to:

$$\sigma_{compton} \propto \frac{Z}{E} \tag{3}$$

  The Compton electron recoil creates the Compton edge, where the electrons have maximum kinetic energy at:

$$T_{max} = E_\gamma \left(1 - \frac{1}{1 + \frac{2E_\gamma}{m_e c^2}}\right) \tag{4}$$

- **Pair production**: In this process the photon is transformed into an electron-positron pair. This process normally involves a nucleus and has a threshold of 1022 keV.
  The cross section of this process is proportional to:

$$\sigma_{e^+e^-} \propto Z^2 \tag{5}$$

During all of these processes a signal is only generated if the energy deposited is equal to or greater than the energy required to create an electron-hole pair and the total number of electron-hole pairs is directly correlated to the total energy deposited, 6.

$$n_{e-h} = \frac{E}{\epsilon} \tag{6}$$

where E is the energy deposited and ϵ is the energy necessary to create a pair.

The large number of electron-hole pairs drift between electrodes, with this drift inducing a charge, 7.

$$Q = n_{e-h} \times q_e \tag{7}$$

where q_e is the electron charge.

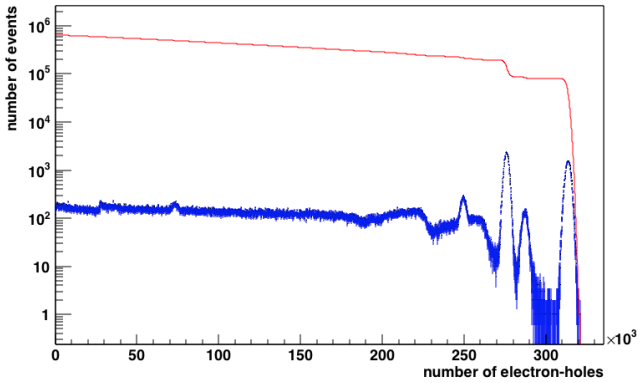

Fig. 2. In blue the number of electron-hole pairs produced by ^{60}Co in 1 mm thick UO_2 is shown. The red line shows the number of registered events for a minimum threshold of number of electron hole pairs. Please note the logarithmic y-axis.

This induced charge then creates a current between the two electrodes, which can be determined using Ramos theorem, 8 ([9]):

$$I = -Q\overrightarrow{v(x)}\overrightarrow{E_Q(x)} \tag{8}$$

with:

$$v = \mu\frac{V_b}{d} \tag{9}$$

where μ is the mobility (electron or hole), V_b is the bias voltage and d is the detector thickness. $E_q = \frac{1}{d}$ is the electric field when one electrode has 1 V and the other one 0.

The device proposed in this work is designed for high dose rate environments and therefore it can be safely assumed that many photons will interact with the sensor matrix per second. A spectrum simulation showing the number of electron-hole pairs produced from the interaction of ^{60}Co with UO_2 is shown in Figure 2.

The device proposed in this work circumvents the slow(er) shaping process that limits normal detectors with the use of fast amplifiers and thresholding. This method allows the number of counts in each detector material above specific threshold values to be counted simultaneously. This is possible in the desired application as there are a limited number (27) of radioisotopes of concern, with each having a specific energy level that can be distinguished, table 2. The energy levels are related to the sources which can be found after nuclear accident or when nuclear plant is in decommisioning.

The validity of this concept has been proven using Monte Carlo simulation. Several different studies (section 3) were performed to determinate how the system can work and which can of energies can be detected.

Material	Energy (keV)
^{60}Co	1173 and 1332
^{241}Am	59
^{137}Cs	661
^{85}Kr	513
^{192}Ir	317, 468 and 604
^{226}Ra	186
^{22}Na	1274
^{131}Ba	123, 216, 373, 496, 620 and 1047
^{68}Ga	1077 and 1883
^{152}Eu	344, 1112 and 1408
^{131}I	284, 364, 636 and 723
^{210}Po	803

TABLE 2
Energy levels for the most common sources which can be found in nuclear power plant.)

One disadvantage of this concept is that it cannot discriminate between a highly active source at a large distance and a lower activity source at a short distance. However, this can be compensated for in the measurement technique by recording data at multiple distances i.e. by having a mobile device.

3 Simulations and Results

The simulations in this work were performed by using Geant4 ([5]). In this simulation the source was located 2 m away from the detectors. The space between the source and detector was filled with air and a 8 μm thick kapton window was placed in front of the detector (figure.3). The detector matrix consisted of a single sensor measuring 5×5 mm, fixed size for all simulations. The thickness was varied between 50 μm and 2 mm.

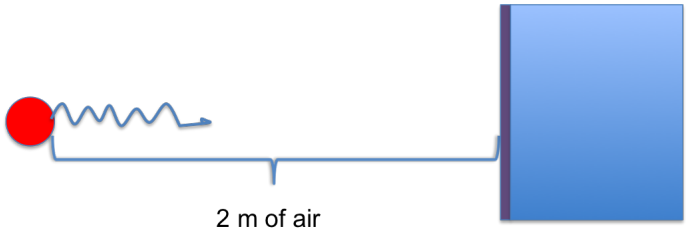

Fig. 3. Schematic of geometry simulation. The source is located 2 m way from the detector. The gap is filled with air and in front of the detector is placed a kapton window.

The spectrum from the simulation of the interaction of 1200 keV gamma rays in 1 mm GaAs detector is shown in figure 4. This shows the three dominant peaks: the photopeak at 1200 keV, the Compton edge at ~1 MeV and a peak at ~200 keV due to pair production. This differs from the spectrum produced by 800 keV gamma rays in the same material, figure 5, as there are only two peaks present, the photopeak at 800 keV and the Compton edge at ~600 keV. The is no lower energy peak as there is insufficient energy for pair production.

Figure 6 and 7 show a similar simulation spectrum for 1200 keV gamma rays but in 1 mm UO_2 rather

that GaAs. Againpeaks from the three process previusly discussed are identify: the photopeak at 1200 keV, the Compton edge at ∼1000 keV and pair production peak at ∼700 keV ($E_\gamma - 0.511$ MeV) and 200 keV. Additionaly there is a peak at ∼1100 keV due to the interaction of the 1200 keV photoelectron electron after emission. The variations in spectra between different detector materials are due to the intrinsic properties of the material, as detailed in table 1.

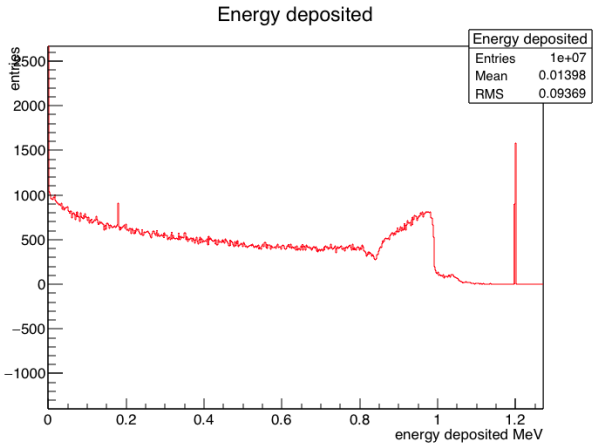

Fig. 4. The spectrum produced by 1.2 MeV gammas in 1 mm of GaAs is shown. At 1.2 MeV is possible to identify the photopeak. At 1 MeV the Compton edge is located, around 0.85 MeV there is a deflection due to the scattering process and around 0.2 MeV the electron produced from the pair production ($E_\gamma - 2 \times 0.511$ MeV).

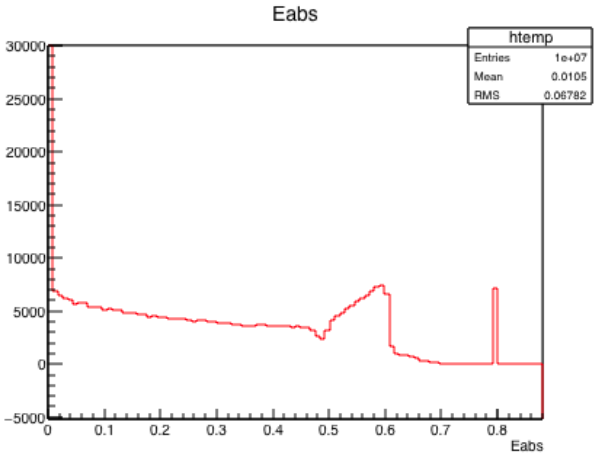

Fig. 5. The spectrum produced by 800 keV gammas in 1 mm of GaAs is shown. At 800 keV is possible to identify the photopeak and at 600 keV the Compton edge.

The first stage of investigation was determining the effect of detector material, detector thickness and incident energy to determine the validity of the simulation. Subsequent simulations studied the detector response to specific radiation energies.

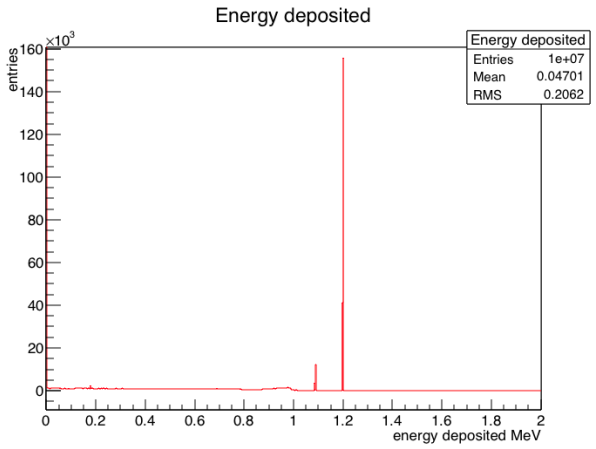

Fig. 6. The spectrum produced by 1.2 MeV gammas in 1 mm of UO_2 is shown.

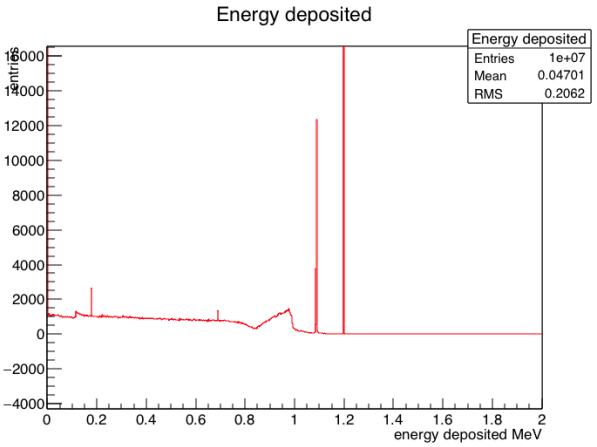

Fig. 7. Focused on UO_2 spectrum which is produced by 1.2 MeV in 1 mm of material. At 1.2 MeV the photopeak is shown, 1.1 MeV is the peak due to the interaction of the electron emetted after the photoelectric interaction, around 1 MeV the Compton edge and just before the scattering process. At ∼0.7 MeV ($E_{gamma} - 0.511$ MeV) and 0.2 MeV the peaks due to the pair production are shown.

A comparison between the deposited energy spectrum and detector thickness for a GaAs detector with 1000 keV is shown in Figure 8. With increasing thickness there is greater attenuation of the gamma rays and hence a greater stopping power of the material. This is evidenced as at 50 μm and 100 μm there is no measureable interaction between the 1000 keV gamma rays and the material. This measurable effect with detector thickness requires the detector thickness, or alternatively detector layering, to be optimised whilst still considering other factors such as cost. Through studying each detector material individually it was found that the optimum thicknesses for a combined mulltidetector system are: 500 μm for silicon; 500 μm for diamond; 1000 μm for UO2 and GaAs; and 2000 μm for CZT.

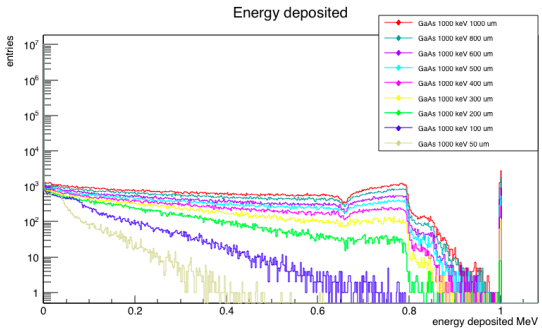

Fig. 8. Deposited energy spectrum for 1 MeV gammas in GaAs layers with different thicknesses. Note that the y-axis is in log scale.

The study was repeated using different energies but the thickness was kept constant at 1000 μm; the results are shown in fig.9. The results show that the photopeak moves in relation to the energy change.

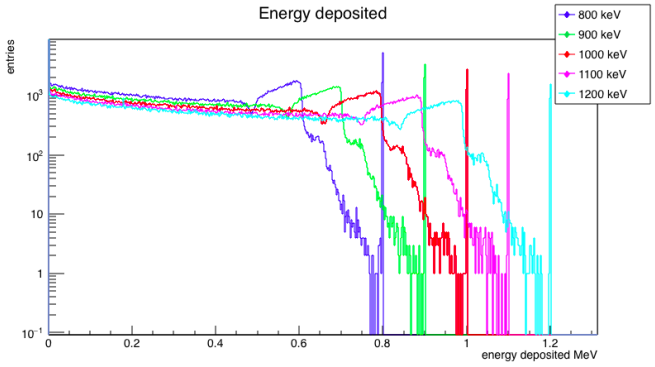

Fig. 9. Energy spectra in 1000 μm GaAs layer with different energies. Note that the y-axis is in log scale.

All the simulation analysis were done using the electron-hole plot.

As each energy band will generate a certain number of electron-hole pairs it will create a peak at a specific location in the electron-hole pair plot. The difference in the number of events before and after the peak can be shown by integration, with the integral value being used to calculate the energy value using equation 6 . Additionally, as each step in the integral plot represents a different energy level it allows the use of thresholding to identify certain peaks in each detector material.

To prove the validity several controls (mystery boxes) where created and the material inside identified.

To make it possible to reconstruct all the energies, *threshold tecnique* was identified.

Figure 10 shows the number of registered events for a minimum threshold of number of electron hole pairs produced when a combination of three different gamma radiation sources (^{241}Am, ^{137}Cs and ^{60}Co) are combined into one source. The jumps in the data correspond to the typical energy lines of the emitted gammas. Considering

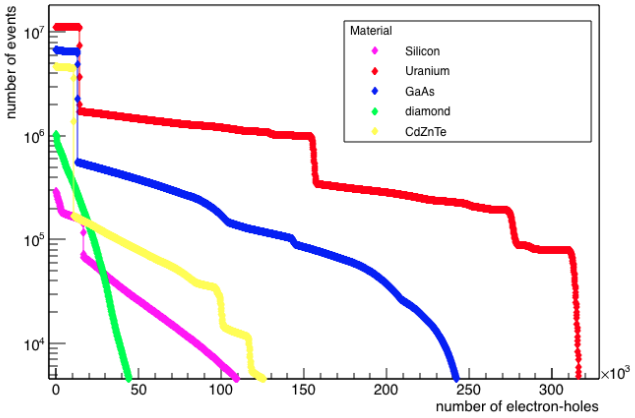

Fig. 10. The number of registered events for a minimum threshold of number of electron hole pairs produced in a mystery box containing 3 different radiation sources: ^{241}Am, ^{137}Cs and ^{60}Co.

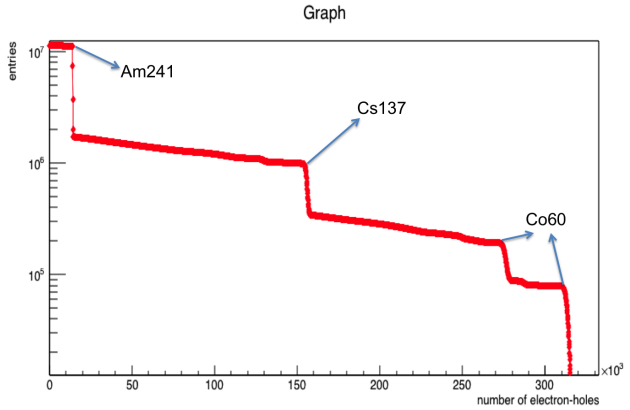

Fig. 11. The number of registered events in 1 mm thick UO_2 for a minimum threshold of number of electron hole pairs produced in a mystery box containing 3 different radiation sources: ^{241}Am, ^{137}Cs and ^{60}Co.

the UO_2 line in figure 10 is possible recognised the different peaks.

In fig 11 the spectra created from the same mistery box in 1 mm thick UO_2 is shown. From the number of electron-hole value is possible reconstruct the energy: ^{241}Am at $\sim$ 13438 (correspond to $\sim$59 keV), ^{137}Cs at $\sim$ 155292 (correspond to $\sim$660 keV) and the two ^{60}Co peaks at $\sim$276106 ($\sim$ 1173 keV) and $\sim$314453 ($\sim$ 1336 keV).

To determinate this peaks, the threshold can be setted in advance in the right range using the MAROC chip.

In fig 12 is shown, in the same condition than before (1 mm thick UO_2), the comparison between dense scan (red line) and the 52 threshold setted (blu line). The jumps, correspond to different energies, in the line are located in the same point than in the red line.

The system is also able to identify different ration in the amount of the materials, how is shown in fig 13. The simulations were done changing the intensity of two

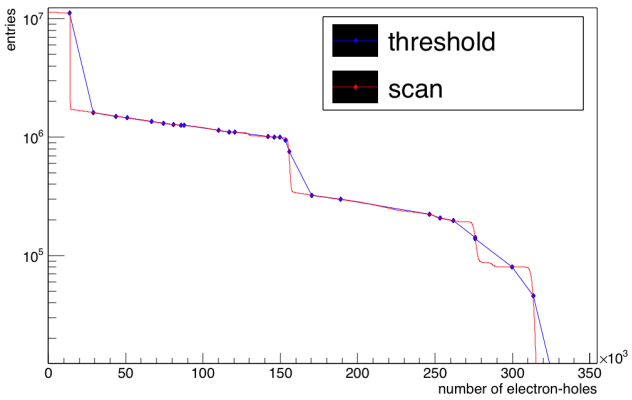

Fig. 12. The number of registered events in 1 mm thick UO_2, the sources are ^{241}Am, ^{137}Cs and ^{60}Co. In red line is shown the result given by a dense scan; otherwise, in blu is shown the result acquired from a 54 thresholds scan.

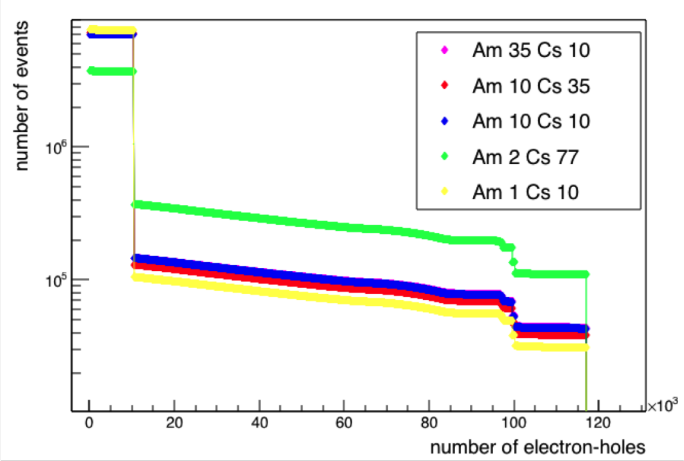

Fig. 13. ^{241}Am, ^{137}Cs in 1 mm thick CdZnte. The ratio of the sources was changed. How is shown, the system is able to detect the different in the material amount.

different sources: ^{241}Am, ^{137}Cs in 1 mm thick CdZnTe. Fig 13 shows the integral value with a dense threshold scan.

4 Readout Design

The proposed concept uses up to 52 discrimination factors over several detector materials, therefore a fast amplifier that has a moderate signal-to-noise ratio for each detector is required. This can be achieved with the use of modern field-programmable gate array (FPGA) chips to record the total counts arising in each threshold bin. The system would also utilise USB communication for system control and data readout.

Readout chain consist of a fast, low noise, charge sensitve preamplifier Amptek A250; amplifier ADA4860 high speed op-amp; FPGA and MARCO3 chip.

First of all the board was tested with several injected signal and the spectra were collected via a multi channel

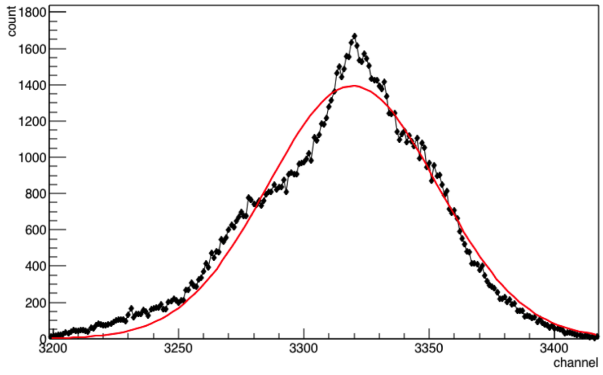

Fig. 14. Output signal results from a 15 mV injected signal.

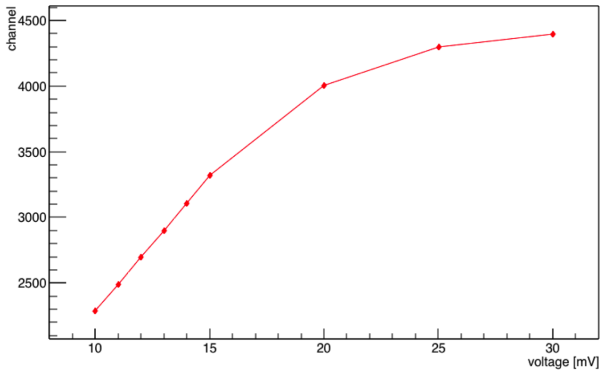

Fig. 15. Voltage scan from 10 mV up to 30 mV. the complete curve is shown.

analyzer. Fig.14 shows the output of 15 mV injected signal in the readout board, the signal is spread across 150 channels. Fig.15 and fig.16 show the voltage scan from 10 mV up to 30 mV. Up to 16 mV linear fit can be applied; for higher voltage the op amp saturates.

Power consumption is also a key point in the readout system. The system required low voltage power supply, high voltage for the bias and electricity supply for the readout system. The energy necessary to work can be equipped via LYPO batteries and via 12 V UAV's power supply.

5 Conclusion

This work presents a novel concept that exploits the differences in the gamma ray interaction cross sections in different detector materials to allow the identification and concentration of radioactive materials in relatively high radiation fields. This can be achieved with the use of a matrix of detectors and the use of thresholding so that only specific energy bins are examined. Simulation results from the concept show good promise and results obtained are highly indicative that such a system would be suitable for use as a fast readout gamma spectrometer

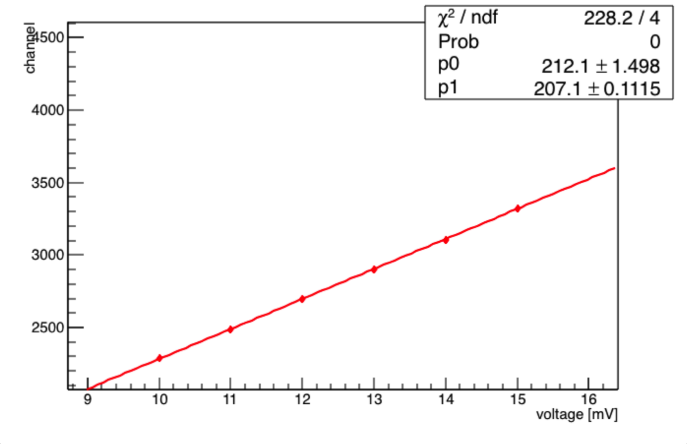

Fig. 16. Linear trend for low level voltage injected.

in high radiation fields. Using 5 different semiconductors allow us to create a flexible system which can be employed in every condition; further more this combination give us the possibility to have a cross check on the online measurement.

REFERENCES

[1] W. R. Leo, *Techniques for Nuclear and Particle Physics Experiments, Second Edition*, Springer.
[2] Salah Awadalla, *Solid-State Radiation Detectors: Technology and Applications*, CRC Press.
[3] K. A. Olive and Others, *Review of Particle Physics.*, Chin. Phys. C, 38(9), 2014.
[4] Lutz, *Semiconductor Radiation Detectors: Device Physics.*, Springer.
[5] S. Agostinelli et al. (Geant4 Collaboration), *Geant4-a simulation toolkit*, NIM A Volume 506, Issue 3, 1 July 2003.
[6] Lots of people, *PDG*, more pdg
[7] Kruschwitz, Craig a. and Mukhopadhyay, Sanjoy and Schwellenbach, David and Meek, Thomas and Shaver, Brandon and Cunningham, Taylor and Auxier, Jerrad Philip, *Semiconductor neutron detectors using depleted uranium oxide*, Proc. SPIE 9213, Hard X-Ray, Gamma-Ray, and Neutron Detector Physics XVI, 92130C .
[8] A. Owens, *Compound Semiconductor Radiation Detectors*, CRC Press.
[9] S. Ramo, *Currents Induced by Electron Motion*, in Proceedings of the IRE, vol. 27, n 9, 1939, pp. 584585 .
[10] Meek, *Semiconductive properties of Uranium Oxides*, Waste Management 2001 Symposium, Tucson, Arizona February 25March 1, 2001.